Combined micro- and nano-scale surface textures for enhanced near-infrared light harvesting in silicon photovoltaics

2011 Nanotechnology 22 095201

(http://iopscience.iop.org/0957-4484/22/9/095201)

Nanotechnology **22** (2011) 095201 (6pp) doi:10.1088/0957-4484/22/9/095201

Combined micro- and nano-scale surface textures for enhanced near-infrared light harvesting in silicon photovoltaics

Chia-Hua Chang[1], Peichen Yu[1], Min-Hsiang Hsu[1], Ping-Cheng Tseng[1], Wei-Lun Chang[2], Wen-Ching Sun[2], Wei-Chih Hsu[2], Shih-Hsin Hsu[3] and Yia-Chung Chang[3]

[1] Department of Photonics and Institute of Electro-Optical Engineering, National Chiao-Tung University, 1001 Ta-Hsueh Road, Hsinchu 300, Taiwan, Republic of China
[2] Green Energy and Environment Research Labs, Industrial Technology Research Institute, 195, Section 4, Chung Hsing Road, Chutung, Hsinchu 310, Taiwan, Republic of China
[3] Research Center for Applied Sciences, Academia Sinica, 128 Academia Road, Section 2 Nankang, Taipei 115, Taiwan, Republic of China

E-mail: yup@faculty.nctu.edu.tw

Received 22 October 2010, in final form 8 December 2010
Published 24 January 2011
Online at stacks.iop.org/Nano/22/095201

Abstract
As silicon photovoltaics evolve towards thin-wafer technologies, efficient optical absorption for the near-infrared wavelengths has become particularly challenging. In this work, we present a solution that employs combined micro- and nano-scale surface textures to increase light harvesting in the near-infrared for crystalline silicon photovoltaics, and discuss the associated antireflection and scattering mechanisms. The surface textures are achieved by uniformly depositing a layer of indium-tin-oxide nanowhiskers on micro-grooved silicon substrates using electron-beam evaporation. The nanowhiskers facilitate optical transmission in the near-infrared by functioning as impedance matching layers with effective refractive indices gradually varying from 1 to 1.3. Materials with such unique refractive index characteristics are not readily available in nature. As a result, the solar cell with combined textures achieves over 90% external quantum efficiencies for a broad wavelength range of 460–980 nm, which is crucial to the development of advanced thin-substrate silicon solar cells.

(Some figures in this article are in colour only in the electronic version)

1. Introduction

Efficient light harvesting plays a key role for solar cells, particularly in crystalline silicon photovoltaics, which now dominate over 80% of the world's production and are evolving towards thin-substrate technologies [1–3]. In conventional crystalline silicon solar cells, artificial micro-grooves suppress the optical reflection loss by introducing multiple reflections on the textures [4], which also serve as light trapping structures by tilting the incident rays to increase the optical path length [5, 6]. However, this technique alone may not be sufficient when the wafer thickness is shrunk below 100 μm, as optical absorption in the infrared becomes particularly challenging [7]. Recent studies have shown that antireflective nanostructures can be tailored for optimal light harvesting, regardless of photon wavelengths, angles of incidence, and polarizations [8–13]. The light trapping effect in nano-scale structures has also been demonstrated in thin film and nanowire solar cells [14–16]. Nevertheless, fabricating nanostructures on crystalline silicon risks an increase in the scattering and surface recombination losses. Moreover, the technologies required to combine both micro- and nano-scale surface textures and the associated advantages have yet been investigated. Herein, we demonstrate an electron-beam evaporation technique that can uniformly cover micro-textured silicon solar cells with a layer of indium-tin-oxide (ITO) nanowhiskers. The nanowhiskers facilitate optical transmission in the near-infrared by functioning as impedance

matching layers with a graded refractive index profile varying from 1 to 1.3. Materials with such unique refractive index characteristics are not readily available in nature. As a result, the solar cell with combined textures achieves over 90% external quantum efficiencies for a broad wavelength range from 460 to 980 nm, which improves significantly over a conventional reference.

2. Experimental details

Previously, we demonstrated the growth of distinctive indium-tin-oxide nanocolumns using oblique electron-beam deposition in an oxygen-deficient atmosphere [17, 18]. The growth involved a two-step process known as nucleation and column growth via surface diffusion [19]. We have found that the oblique incident vapor reduces the flux density of molecules on the surface which facilitates the separation and formation of nuclei. Moreover, the oxygen deficiency allows the segregation of tin-doped indium to form a liquid surface that promotes the absorption of incident vapors, resulting in vertical column growth. The self-catalytic vapor–liquid–solid growth mechanism dictates the structural and material properties of the indium-tin-oxide nanostructures [20, 21]. Such a deposition technique can be directly applied to conventional silicon solar cells without tilting the substrate, as the alkaline-solution-etched textures naturally form a tilted surface at 54.7°.

In this work, the fabrication of solar cells follows standard procedures. First, p-type Si ⟨100⟩ wafers were etched by a potassium hydroxide solution (KOH:H_2O = 1:1) at 80 °C for 40 min for saw damage etch and texture etch. The microscale surface textures formed a tilted angle of ∼50.5° with respect to the horizontal plane. Next, a 500 nm thick n-type layer was created on the textured surface by phosphorus diffusion using $POCl_3$ in a Centrotherm tube furnace at 850 °C for 1 h, forming the p–n junction interface. The surface was then passivated with an 80 nm thick SiN_x layer, which was deposited in a Centrotherm direct-plasma PECVD furnace at 400 °C for 30 min. The front and back metallization were screen-printed with conductive pastes using a semi-automatic printer (ATMASC 25PP). The indium-tin-oxide nanowhiskers were then deposited using electron-beam evaporation before contact firing. The nanowhiskers were deposited on the micro-grooved surface using electron-beam evaporation. The target source contained 5 wt% SnO_2 and 95 wt% In_2O_3. At the beginning of the evaporation, the chamber pressure was first pumped down to $\sim 10^{-6}$ Torr, followed by the introduction of a nitrogen flow rate at 1 sccm. During growth, the chamber was stabilized at 260 °C and $\sim 10^{-4}$ Torr with a deposition rate of 0.15 nm s^{-1} for deposition times of 9, 27, and 45 min. The electrode co-firing step was performed in a fast-firing belt furnace at a peak temperature of 800 °C. Finally, the edge isolation was achieved using a 532 nm Nd:YAG laser. The fabricated device has an area of 2.3 × 3.5 cm^2. However, the deposition technique has proven to be uniform up to an area of 10 × 10 cm^2.

The reflectance and haze ratio was measured by UV–VIS–NIR spectrophotometer (Hitachi U-4100). The current–voltage characteristics of fabricated solar cells were performed under a simulated AM1.5G (Air Mass 1.5, Globe) illumination condition. The power conversion efficiency (PCE) measurement system consisted of a power supply (Newport 69920), a 1000 W Class A solar simulator (Newport 91192A) with a Xe-lamp and an AM1.5G filter, a probe stage, and a source-meter (Keithley 2400) with a four-wire mode. The spectrum of the solar simulator was measured by a calibrated spectroradiometer (Soma S-2440) in the wavelength range of 300–1100 nm. A mono-crystalline silicon reference cell (VLSI Standards, Inc.) was used for solar simulator calibration before measurement [22]. The mismatch factor (M) was 0.9965, calculated using the spectral response of the reference cell and the cell under test, the spectrum of the solar simulator, and the ASTM G173-03 reference spectrum [23, 24].

3. Results and characterization

As can be seen in figure 1(a), the scanning electron micrograph (SEM) shows that the textured surfaces are uniformly covered with whisker structures on all sides, down to the grooves, which is also revealed by the cross-sectional SEM image shown in figure 1(b). Photographs taken for devices with the conventional antireflection treatment of an 80 nm thick SiN_x coating on the micro-grooves and with ITO nanowhiskers grown for 27 min are shown in figures 1(c) and (d), respectively. By comparing figures 1(c) and (d), we note that the cell with the whisker structures appears nearly black, in contrast to the blue surface of the reference device, due to reduced optical reflection for visible wavelengths.

The reflectance characteristics depend highly on the profiles, heights, and densities of ITO nanostructures. With different deposition conditions, the microscale grooves could be uniformly covered with nanocolumns or nanowhiskers of various densities. Figures 2(a)–(c) show the cross-sectional SEMs of ITO nanostructures grown on passivated, micro-textured silicon substrates for 9, 27, and 45 min. The corresponding tilted top-view images are shown in figures 2(d)–(f), respectively. For a short deposition time of 9 min, randomly oriented nanocolumns are formed with an average thickness of ∼200 nm. The density and thickness are relatively low compared to structures that are grown for a longer time. When increasing the deposition time, the columns stop growing vertically at a height of ∼720 nm, and become thicker with branches appearing on their sides. Further increases in deposition time give rise to denser whisker structures with multiple branches, as shown in figures 2(c) and (f). The respective reflectance spectra of the devices in figure 2 are plotted in figure 3(a). The spectra were measured by an integrating sphere, which included the specular and diffuse components of optical reflection, corresponding to the zeroth and higher-order optical diffractions respectively [25]. We note that the specular reflection of micro-textured silicon substrates is generally minimized due to a strong optical absorption. Therefore, the reflection loss measured by the integrating sphere is dominated by backward scattering. As seen in figure 3(a), the nanocolumns grown for 9 min exhibit low reflection in the ultraviolet/blue wavelengths, but relatively high reflection in the near-infrared. Such characteristics

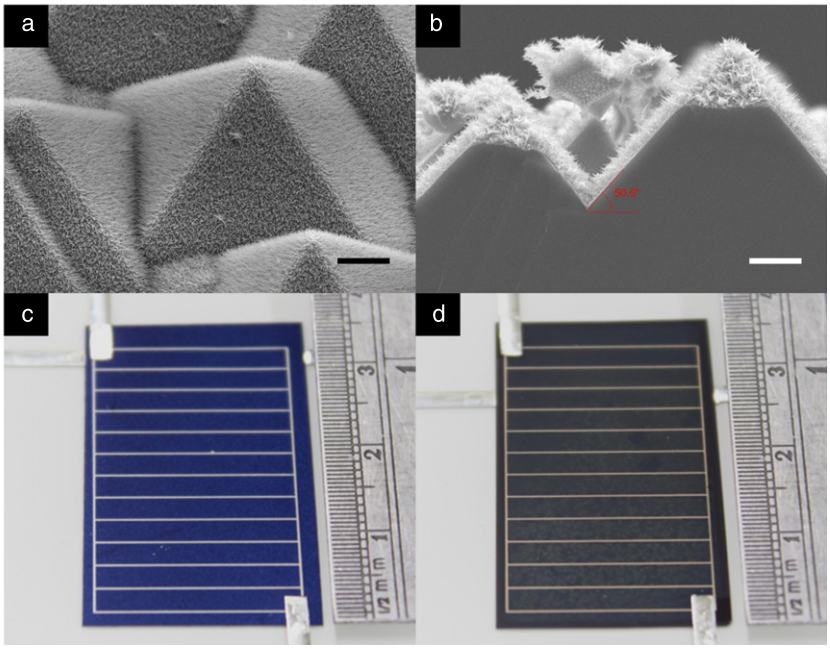

Figure 1. Scanning electron micrographs of indium-tin-oxide nanowhiskers deposited on a passivated, micro-grooved silicon solar cell: (a) tilted top view and (b) cross-sectional view. The scalar bars are 4 μm in length. (c) Photographs of a conventional crystalline silicon solar cell, and (d) adding indium-tin-oxide nanowhiskers grown for 27 min; showing blue and black surface colors at a tilted angle, respectively.

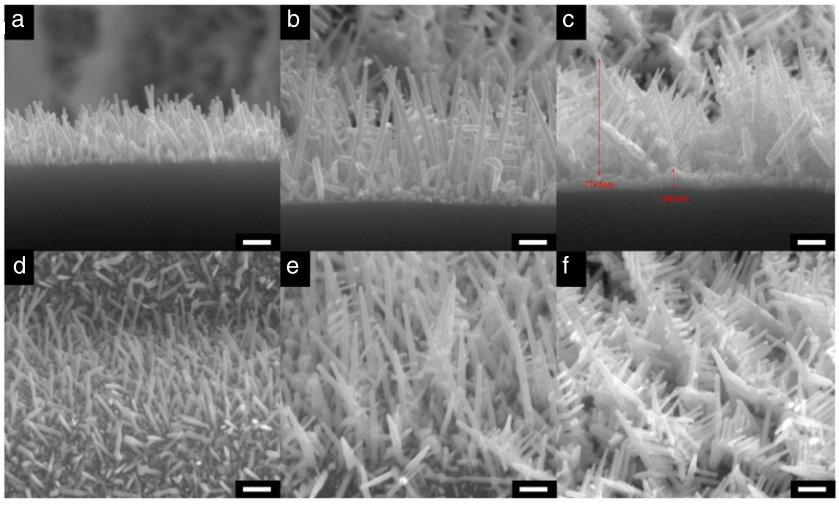

Figure 2. Cross-sectional scanning electron micrographs of indium-tin-oxide nanowhiskers grown at different deposition times: (a) 9 min, (b) 27 min and (c) 45 min on passivated, micro-grooved silicon surfaces. (d)–(f) are the corresponding tilted surface top views of (a)–(c), respectively. The scalar bars are 200 nm in length.

are opposite to the dense whiskers grown for 45 min. In general, the antireflective properties of uniformly distributed nanostructures are best described by the effective-medium theory, where the constitutive air volume depicts the material dispersion [26–29]. Predictably, a growth period of between 9 and 45 min could result in low reflection for both short and long wavelengths, which is confirmed by nanowhiskers grown for 27 min. In order to compare the modified surface structures with existing technology, figure 3(b) shows the reflectance spectra of a bare textured silicon substrate, the same substrate with an 80 nm thick SiN_x antireflection coating, and with both 80 nm thick SiN_x (for passivation) and ITO nanowhiskers grown for 27 min. As seen in figure 3(b), the first two have a relatively high reflectance in the ultraviolet and near-infrared wavelength ranges, while the reflectance for the ITO nanowhiskers is significantly reduced (<5%) from 350 to 1200 nm.

An analytical or numerical optical model that simultaneously describes the optical properties of nanostructures on micro-textures is difficult, as the geometric dimensions span over three orders of magnitude. It is generally accepted that ray-tracing is applicable to micro-textures as the dimensions

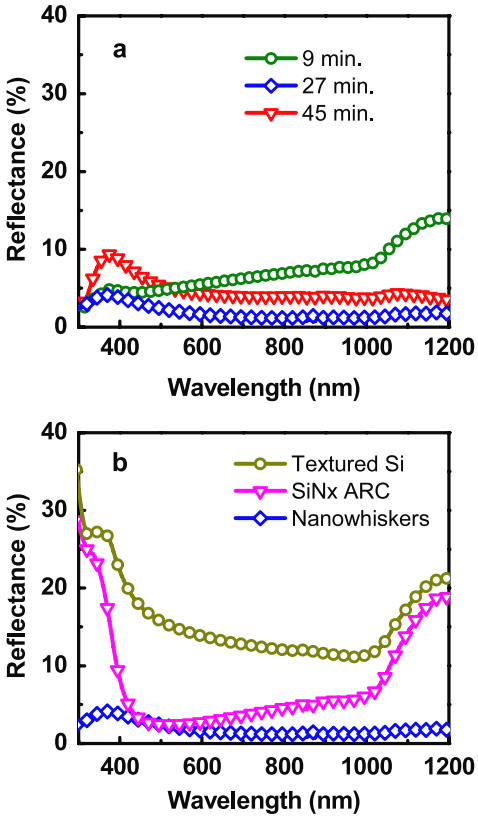

Figure 3. (a) The reflectance spectra of indium-tin-oxide nanowhiskers on passivated, micro-grooved silicon surfaces for various deposition times: 9, 27, 45 min. (b) The reflectance spectra of a conventional micro-grooved silicon substrate, with an 80 nm thick SiN_x antireflection coating, and with both 80 nm thick SiN_x (for passivation) and indium-tin-oxide nanowhiskers (27 min). The spectra were measured by an integrating sphere.

involved are at least one order of magnitude larger than the incident photon wavelengths. Therefore, the optical properties of micro-textures can be understood using geometric optics with a tilted surface normal [30, 31]. Under this simplification, the optical characteristics of ITO nanowhiskers can be further investigated by oblique deposition (at 55°) on a flat substrate, where both ITO film coated glasses and flat silicon substrates are used. Using the previously described deposition conditions, the resulting structures are very similar to those shown in figure 2, as the growth mechanism depends little on the substrate type. The optical haze ratio, defined as the diffused transmittance to the total transmittance is plotted in figure 4 for three different deposition times: 9, 27, and 45 min. The diffused transmittance is a direct result of forward scattering due to surface roughness [32, 33]. As shown in figure 4, the nanowhiskers show marked haze ratios for wavelengths up to 600 nm, which can be correlated to the surface morphology. The strong forward scattering is favorable in thin silicon photovoltaics due to the increase in optical absorption path lengths for the visible light. For comparison, a referenced ITO film has haze ratios between 1% and 0.1%, indicating very little diffuse transmission induced by the film. Moreover, the haze ratio is nearly negligible for wavelengths >600 nm, implying that the nanowhisker layer behaves as a thin film for

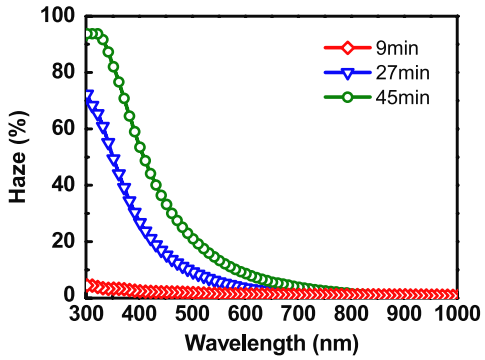

Figure 4. The optical haze ratio as a function of wavelengths for indium-tin-oxide (ITO) nanostructures grown with various deposition times: 9, 27, 45 min.

long wavelengths. Accordingly, an optical model based on ellipsometry characterization is established in order to reveal the thin film behavior of the nanowhisker layer.

Figure 5(a) shows the spectral reflectance of ITO nanowhiskers grown for 27 min on a flat silicon substrate with an 80 nm thick SiN_x passivation layer for s- and p-polarized light incident at 30°, as illustrated in the inset. Without the micro-grooves, the specular reflection is large enough to be detected. As seen in figure 5(a), the reflectance is less than 10% from the 600 to 1100 nm wavelengths, and also relatively polarization-insensitive. Model calculations based on ellipsometry analysis are also plotted for comparison. The optical model can well describe the nanowhisker behavior for wavelengths larger than 600 nm at various angles of incidence and for both polarizations. Discrepancies only arise for shorter wavelengths due to increased scattering. Figure 5(b) shows the calculated optical model at 600 nm wavelength obtained by fitting the spectroscopic ellipsometry results over a spectral range of 600–2000 nm at five angles of incidence (55°, 60°, 65°, 70°, and 75°). The model fitting is carried out using a commercial implementation WVASE32 (J A Woollam Co.), where the nanowhisker layer is modeled as a graded index layer with varying porosities along the vertical direction using an effective-medium approximation (EMA) [34]. The horizontal axis represents the thickness of layers deposited on the flat silicon substrate, where the origin is chosen to be at the silicon/SiN_x interface. The silicon substrate and the SiN_x passivation layer, denoted as layers A and B in figure 5(b) respectively, are separately characterized for thicknesses and dispersion relations, and therefore are directly inserted into the model. Figure 5(b) reveals that the nanowhisker layer is optically equivalent to a stack of two dielectric layers: the bottom one with a constant refractive index of 1.45 (layer C), and the top one with graded refractive indices varying from 1.0 to 1.3 (layer D). We note that the attenuation coefficient shown in figure 5(b) is higher than that of an ITO thin film ~0.003 and could be overestimated, presumably arising from the scattering loss. However, the ITO material indeed has a parasitic absorption for wavelengths below 400 nm which impacts the solar cell characteristics slightly [35]. The variable-angle spectroscopic ellipsometry analysis is consistent with the SEM observation as the bottom nanowhiskers contain

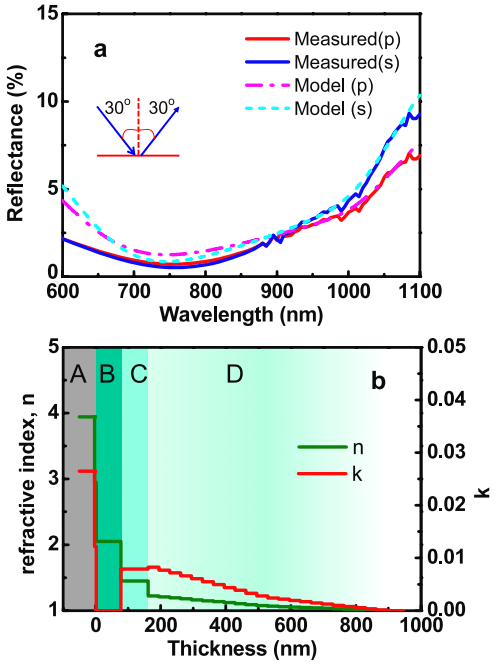

Figure 5. (a) The spectral reflectance of indium-tin-oxide nanowhiskers grown for 27 min on a flat and passivated silicon substrate and the corresponding model fits for both s- and p-polarizations at an incident angle of 30° (inset). (b) The dispersion and attenuation coefficient of indium-tin-oxide nanowhiskers as a function of the thickness obtained from the model fitting of (a) at 600 nm wavelength.

randomly positioned nucleation cores and short rods with assorted dimensions and therefore should be relatively dense. On the other hand, the top whisker structures are relatively airy, and the graded index profile may result from the gradual change of the air volume ratio though out the structures, as seen in figure 2(b). The graded and step refractive index profiles shown in figure 5(b) facilitate optical transmission, with the nanowhiskers functioning as impedance matching layers between air and semiconductors to improve the optical absorption of the crystalline silicon solar cells for wavelengths above 600 nm.

The current–voltage characteristics of silicon solar cells with an 80 nm thick SiN_x antireflection coating and with both SiN_x and ITO nanowhiskers (27 min), denoted as the reference cell and the whisker cell respectively, are summarized in table 1. The nanowhisker structures increase the short-circuit current density by an additional 1.52 mA cm^{-2}, and the power conversion efficiency by 1.1%. As seen in figure 6, such an improvement is mostly contributed to by enhanced photoelectric conversion for wavelengths larger than 600 nm. The external quantum efficiency (EQE) achieves more than 90% for a broad wavelength range from 460 nm to 980 nm, showing a significant improvement over the conventional reference. However, the high quantum efficiency in the near-infrared could have resulted from either or both, efficient optical absorption and effective carrier collection. Therefore, we have confirmed that the improvement solely arises from the former due to nearly identical internal quantum efficiency (IQE) spectra, obtained by dividing the

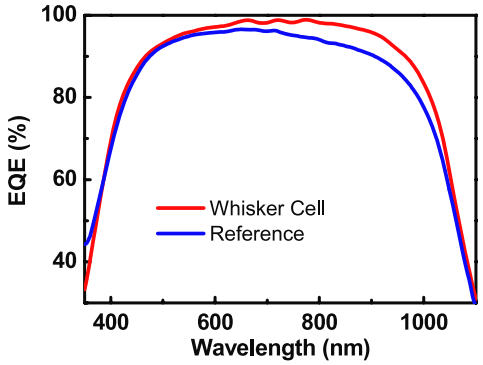

Figure 6. The measured external quantum efficiency (EQE) of a conventional silicon solar cell (the reference) and the cell with indium-tin-oxide nanowhiskers grown for 27 min (the whisker cell).

Table 1. Current–voltage characteristics under a simulated AM1.5G illumination condition.

Device	J_{sc} (mA cm^{-2})	V_{oc} (V)	FF (%)	PCE (%)
Reference	35.84	0.610	73.45	16.08
Whisker cell	37.36	0.612	75.13	17.18

EQE with the absorption spectra calculated from figure 3(b). Although the solar cell with combined textures is implemented on a relatively thick substrate (230 μm), the absorption enhancement due to antireflection in the near-infrared is already evident. The light trapping effects should be further investigated in thin-wafer cells.

4. Conclusion

In conclusion, we demonstrate a viable solution to enhance near-infrared light harvesting using combined micro- and nano-scale surface textures on a crystalline silicon solar cell. The broadband optical transmission is facilitated by indium-tin-oxide nanowhisker structures which serve as impedance matching layers between air and semiconductors. As a result, the solar cell with combined textures achieves over 90% external quantum efficiencies for a broad wavelength range from 460 to 980 nm. The nanowhiskers also provide strong forward scattering for ultraviolet and visible light, which is crucial in thin-wafer silicon photovoltaics to increase the optical absorption path.

Acknowledgments

The authors thank Professor H C Kuo at the Department of Photonics, National Chiao-Tung University for facility support. This work was founded by the National Science Council in Taiwan under grant number NSC96-2221-E-009-092-MY3, NSC 98-2112-M-001-022-MY3 and the Bureau of Energy and Ministry of Economic Affairs in Taiwan.

References

[1] Yole Dévelopment 2008 Photovoltaic fab database www.yole.fr/pagesAn/products/pvd.asp

[2] Fath P, Keller S, Winter P, Jooss W and Herbst W 2009 Status and perspective of crystalline silicon solar cell production *Proc. 34th IEEE Photovoltaic Specialists Conf. (Philadelphia, PA, June 2009)* Institute of Electrical and Electronics Engineers, pp 2471–6

[3] Glunz S W 2007 High-efficiency crystalline silicon solar cells *Adv. Opto-Electron.* **2007** 97370

[4] Baraona C R and Brandhorst H W 1975 V-grooved silicon solar cells *Proc. 11th IEEE Photovoltaic Specialists Conf. (Phoenix, AZ, May 1975)* Institute of Electrical and Electronics Engineers, pp 44–8

[5] Yablonovitch E and Cody G D 1982 Intensity enhancement in textured optical sheets for solar cells *IEEE Trans. Electron. Devices* **29** 300

[6] Campbell P 1993 Enhancement of light absorption from randomizing and geometric textrures *J. Opt. Soc. Am.* B **10** 2410

[7] Tsunomura Y, Yoshimine Y, Taguchi M, Baba T, Kinoshita T, Kanno H, Sakata H, Maruyama E and Tanaka M 2009 Twenty-two percent efficiency HIT solar cell *Sol. Energy Mater. Sol. Cells* **93** 670–3

[8] Huang Y F *et al* 2007 Improved broadband and quasi-omnidirectional antireflection properties with biomimetic silicon nanostructures *Nat. Nanotechnol.* **2** 770–4

[9] Xi J Q, Schubert M F, Kim J K, Schubert E F, Chen M, Lin S Y, Liu W and Smart J A 2007 Optical thin-film materials with low refractive index for broadband elimination of Fresnel reflection *Nat. Photon.* **1** 176–9

[10] Chiu C H, Yu P, Chang C H, Yang C S, Hsu M H, Kuo H C and Tsai M A 2009 Oblique electron-beam evaporation of distinctive indium–tin-oxide nanorods for enhanced light extraction from InGaN/GaN light emitting diodes *Opt. Express* **17** 21250–6

[11] Chang C H, Yu P and Yang C S 2009 Broadband and omnidirectional antireflection from conductive indium–tin-oxide nano-columns prepared by glancing-angle deposition with nitrogen *Appl. Phys. Lett.* **94** 051114

[12] Lalanne L and Morris G M 1997 Antireflection behavior of silicon subwavelength periodic structures for visible light *Nanotechnology* **8** 53–6

[13] Kanamori Y, Hane K, Sai H and Yugami H 2001 100 nm period silicon antireflection structures fabricated using a porous alumina membrane mask *Appl. Phys. Lett.* **78** 142–3

[14] Zhu J, Hsu C M, Yu Z, Fan S and Cui Y 2010 Nanodome solar cells with efficient light management and self-cleaning *Nano Lett.* **10** 1979–84

[15] Kelzenberg M D, Boettcher S W, Petykiewicz J A, Turner-Evans D B, Putnam M C, Warren E L, Spurgeon J M, Briggs R M, Lewis N S and Atwater H A 2010 Enhanced absorption and carrier collection in Si wire arrays for photovoltaic applications *Nat. Mater.* **9** 239–44

[16] Garnett E C and Yang P 2008 Silicon nanowire radial p–n junction solar cells *J. Am. Chem. Soc.* **130** 9224–5

[17] Yu P, Chang C H, Chiu C H, Yang C S, Yu J C, Kuo H C, Hsu S H and Chang Y C 2009 Efficiency enhancement of GaAs photovoltaics employing indium–tin-oxide nano-columns *Adv. Mater.* **21** 1618–21

[18] Peng X S, Meng G W, Wang X F, Wang Y W, Zhang J, Liu X and Zhang L D 2002 Synthesis of oxygen-deficient indium–tin-oxide (ITO) nanofibers *Chem. Mater.* **14** 4490–3

[19] Takaki S, Aoshima Y and Satoh R 2007 Growth mechanisms of indium tin oxide whiskers prepared by sputtering *Japan. J. Appl. Phys.* **46** 3537–44

[20] Yumoto H, Sako T, Gotoh Y, Nishiyama K and Kaneko T J 1999 Growth mechanism of vapor–liquid–solid (VLS) grown indium tin oxide (ITO) whiskers along the substrate *J. Cryst. Growth* **203** 136–40

[21] Chen Y Q, Jiang J, Wang B and Hou J G 2004 Synthesis of tin-doped indium oxide nanowires by self-catalytic VLS growth *J. Phys. D: Appl. Phys.* **37** 3319–22

[22] Emery K and Osterwald C 1989 Solar cell calibration methods *Sol. Cells* **27** 445–53

[23] Air Mass 1.5 Solar Spectral Irradiance http://rredc.nrel.gov/solar/spectra/am1.5

[24] Emery K A, Osterwald C R, Cannon T W, Myers D R, Burdick J, Glatfelter T, Czubatyj W and Yang J 1985 Methods for measuring solar cell efficiency independent of reference cell or light source *Proc. 18th IEEE Photovoltaic Specialists Conf. (Las Vegas, NV, Oct. 1985)* Institute of Electrical and Electronics Engineers, pp 623–8

[25] Ginneken B V, Stavridi M and Koenderink J J 1998 Diffuse and specular reflectance from rough surface *Appl. Opt.* **37** 130–9

[26] Tinga W R, Voss W A G and Blossey D F 1973 Generalized approach to multiphase dielectric mixture theory *J. Appl. Phys.* **44** 3897–902

[27] Chen H Y, Lin H W, Wu C Y, Chen W C, Chen J S and Gwo S 2008 Gallium nitride nanorod arrays as low-refractive-index transparent media in the entire visible spectral region *Opt. Express* **16** 8106–16

[28] Aspnes D E 1982 Optical properties of thin films *Thin Solid Films* **89** 249–62

[29] Smith D R, Padilla W J, Vier D C, Nemat-Nasser S C and Schultz S 2000 Composite medium with simultaneously negative permeability and permittivity *Phys. Rev. Lett.* **84** 4184–7

[30] Chiao S C, Zhou J L and Macleod H A 1993 Optimized design of an antireflection coating for textured silicon solar cells *Appl. Opt.* **32** 5557–60

[31] Zhao J and Green M A 1991 Optimized antireflection coatings for high-efficiency silicon solar cells *IEEE Trans. Electron Devices* **38** 1925–34

[32] Baik S J, Jang J H, Lee C H, Cho W Y and Lim K S 1997 Highly textured and conductive undoped ZnO film using hydrogen post-treatment *Appl. Phys. Lett.* **70** 3516–8

[33] Zeman M, Swaaij R A C M M V, Metselaar J W and Schropp R E I 2000 Optical modeling of a-Si:H solar cells with rough interfaces: effect of back contact and interface roughness *J. Appl. Phys.* **88** 6436–43

[34] Hsu S H, Liu E S, Chang Y C, Hilfiker J N, Kim Y D, Kim T J, Lin C J and Lin G R 2008 Characterization of Si nanorods by spectroscopic ellipsometry with efficient theoretical modeling *Phys. Status Solidi* a **205** 876–9

[35] Kim H, Gilmore C M, Piqué A, Horwitz J S, Mattoussi H, Murata H, Kafafi Z H and Chrisey D B 1999 Electrical, optical, and structural properties of indium–tin-oxide thin films for organic light-emitting devices *J. Appl. Phys.* **86** 6451–61